(Preprint) AAS 26-891

USING ELECTROSTATIC TORQUES TO MANAGE ANGULAR MOMENTUM WITH UNCONTROLLED ROTATING TARGETS

James D. Walker III* and Hanspeter Schaub†

De-saturation maneuvers are required for long term space missions to prevent reaction wheels from exceeding their maximum wheel speed. These are typically performed with chemical thrusters. However, thruster maneuvers are limited by the amount of propellant carried by the satellite. This work presents an alternative method using Coulomb torques suitable for the geosynchronous environment. Significant electrostatic torques are generated between electrically charged servicing and target spacecraft. By controlling the relative attitude of the two charged non-spherical objects, these torques can be manipulated to act opposite the stored angular momentum vector of the servicer, thus applying an external torque to spin down its reaction wheels. This paper investigates the effect of a rotating target on these electrostatic momentum management maneuvers. For the spacecraft configurations considered here, it is found that while thrusters may still be required, electrostatic momentum management can reduce the frequency of de-saturation burns, significantly extending missions operating under propellant constraints. Additionally, it is shown that the most important factor for achieving consistent electrostatic torques is the servicer's attitude: accentuating the asymmetry of the servicer relative to the target makes the electrostatic momentum management maneuvers robust to rotating spacecraft.

INTRODUCTION

Electrostatic actuation (EA) is a novel method for contactless manipulation of the relative motion of nearby spacecraft through electrostatic forces and torques. When exposed to the energetic plasma of the space environment, the conducting surfaces of satellites acquire non-zero electric potentials.[1] As charged spacecraft approach one another, they exert Coulomb forces and torques on the other object.[2,3] These electrostatic perturbations allow a spacecraft to touchlessly manipulate the relative motion of another, expanding proximity and rendezvous operations as relative motion maneuvers can be performed without docking or expending propellant.[4–6]

Coulomb formation flying is an EA technique that allows a formation of satellites to be maintained using these forces.[3] For a collection of charged spacecraft, station-keeping maneuvers can be performed by controlling the electric potential on individual spacecraft in the formation. By using electrostatic forces to maintain the formation, propellant costs are reduced, thus extending mission lifetimes. This EA maneuver requires each spacecraft to control its own potential; however some techniques are applicable for uncontrolled spacecraft. Electrostatic detumbling can be used to spin

*NDSEG Fellow and Graduate Research Assistant, Ann and H.J. Smead Department of Aerospace Engineering Sciences, University of Colorado Boulder, Colorado Center for Astrodynamics Research, Boulder, CO, 80303 USA. James.WalkerIii@colorado.edu

†Distinguished Professor, Schaden Leadership Chair, Ann and H.J. Smead Department of Aerospace Engineering Sciences, Colorado Center for Astrodynamics Research. AAS Fellow, AIAA Fellow

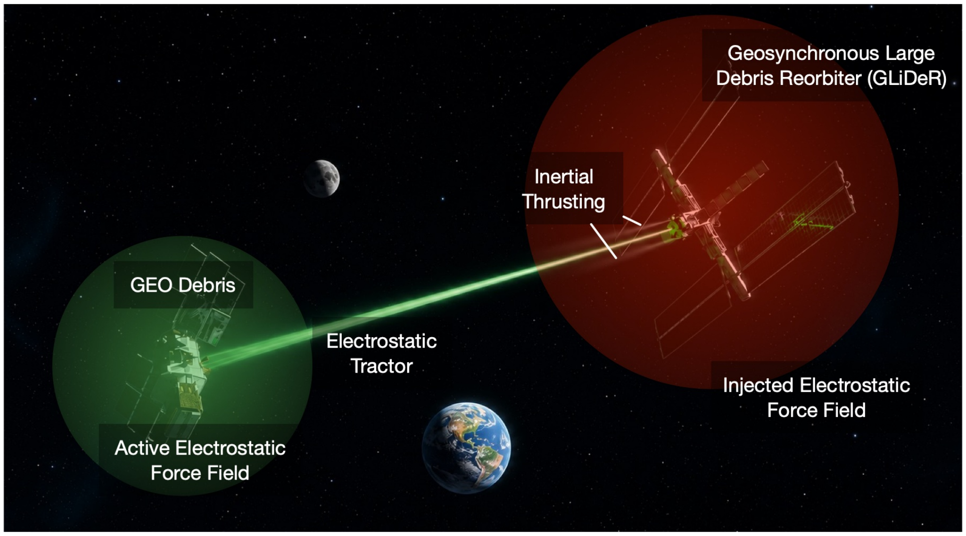

Figure 1. Conceptual representation of a servicer tugging geostationary debris using the Electrostatic Tractor method.

down tumbling debris objects.[7–9] By driving the electric potential of the target object to be either positive or negative, the electrostatic torques generated between the two objects can be controlled. Generating a torque that acts in the direction opposite the target's angular momentum vector reduces the target's angular velocity, making docking to the object safer.[7,10,11] Finally, the electrostatic tractor is a special case of Coulomb formation flying for debris removal in Geostationary orbits.[12–14] Using an electron beam to charge the target negatively and the controlled servicing spacecraft positively, an attractive Coulomb force is generated between the two objects.[15,16] The servicer utilizes this "electrostatic tractor" to tug the debris object to a higher, graveyard orbit where it will no longer interact with GEO satellites. Figure 1 shows a concept figure of this debris removal technique.

For electrostatic forces and torques to be large enough, these maneuvers are performed over a few spacecraft radii (10's of meters) separation distance with electric potentials up to 10's of kilovolts.[17] The separation distance is maintained using a relative motion controller informed by the electrostatic perturbations.[18] Methods for actively controlling an uncontrolled target's potential have been developed and validated experimentally,[19,20] but these large potentials are only achievable in high orbits where the plasma is sparse, like GEO.[1,21,22] One concern that arises is the continual buildup of angular momentum caused by the significant electrostatic torques experienced during these maneuvers. The spacecraft must have large potentials to generate significant force between them, but this also leads to large electrostatic torques. These torques must be stored by momentum exchange devices in order to maintain attitude control authority. Reaction wheels are most commonly used on spacecraft: the wheels spin up, storing the increasing angular momentum. This solution allows spacecraft to maintain attitude control while experiencing external torques, but eventually the wheels will saturate. There is a maximum speed reaction wheels can achieve and once they achieve this speed, the spacecraft will begin to drift about that axis. The target object, i.e. debris, has no active attitude control system and will naturally spin up during the e-tractor operations.

Servicer de-saturation maneuvers are performed to combat reaction wheel saturation. The wheel speeds are reduced by applying an external torque to the spacecraft in the direction opposite the stored angular momentum. For low altitude satellites, magnetorquers are a common method to apply the external torque:[23–26] the spacecraft leverage a torque against the magnetic field of the Earth. At higher altitude orbits, like GEO where EA is applicable, chemical thrusters are primarily used.[27] Thruster burns are performed to apply the external torque, but this limits the lifetime of the satellite to the fuel required for these maneuvers. Electrostatic momentum management (EMM) is a novel method of angular momentum management that reduces the fuel costs of electrostatic actuation maneuvers.[28]

Electrostatic torques are dependent on the geometry of the two spacecraft as well as their relative attitude. The idea of EMM is to manipulate the relative attitude to generate an electrostatic torque that acts in the direction opposite the stored angular momentum of the servicer.[28] The servicer maintains the first attitude while the reaction wheels spin up to account for the electrostatic torque. Once the wheel speeds reach a threshold, the spacecraft slews to a new attitude where the torques acts in the opposite direction. This attitude is maintained until the angular momentum is removed, at which point the spacecraft slews back to the first attitude. With this concept, much of the angular build-up of the servicer is transferred onto the already tumbling debris object.

Preliminary analysis demonstrated the ability to build a database of torques the servicer will experience and then searcher said database for attitude required to generate the torque most anti-parallel to an input vector. By rotating between the two attitudes, the buildup of angular momentum can be delayed.[28] This prior work has focused on the feasibility of this maneuver, only considering the generated torques and assuming a rotationally fixed target.[28] This assumption is only applicable when both the servicer and target are controlled, like for Coulomb formation flying. However, for the electrostatic tractor where the debris object is uncontrolled, the generated torques will cause the object to rotate.

This paper aims to fill this gap by considering a free floating targt: starting at rest, the debris experiences an electrostatic torque and begins to rotate. This means that the torque at the second attitude will not be the exact precomputed torque and can lead to a continual buildup of angular momentum. This is the first paper to consider EMM with uncontrolled targets rotations as well the first to characterize the relationship between these rotations and the generated torques. The servicer's relative attitude plays a major role in torque generation and is used as the mechanism in which this buildup is explored. Specifically, the distribution of possible torques is computed for a variety of servicer attitudes. Through this analysis, a relationship between servicer symmetry and the range of the torque distribution is revealed.

This paper is organized as follows: first, the method for computing the torque database is presented, followed by a description of the guiding principals of electrostatic momentum management. Numerical simulations are then conducted to evaluate the effect of a rotating target. The first analysis presents a test scenario with a servicing maintaining a fixed separation from a highly charged target for both short term and long term maneuvers. For the same scenario, the ability of the target to manage pure torques about the principle axes is then determined. Finally, this work is expanded to evaluate a variety of servicer attitudes and the torques generated by a target with arbitrary attitude.

NUMERICAL METHODS

Electrostatic Force and Torque Modeling

In order to build a database of torques, the Multi-Sphere Method (MSM) is used to approximate the electrostatic torques between the two spacecraft. The MSM is a method for rapidly computing the electrostatic forces and torques between charged objects for use in dynamic simulations. By

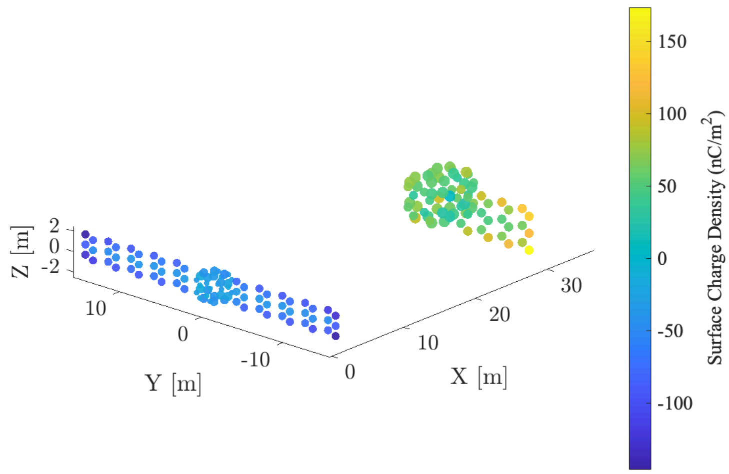

Figure 2. The Multi-Sphere Method representation of both spacecraft

discretizing the objects as a collection of spheres the charge on each sphere can be estimated rapidly. The spheres' size and location are chosen to accurately represent the electric field generated by the object. Other methods typically use finite element analysis to determine the charge of a spacecraft surface, however these are much too slow for faster-than-real-time dynamics modeling. It was found that using MSM, the generated forces and torques can be determined within a 1% accuracy of FEAs. The development of MSM and the optimal sphere selection is presented in Refs. 29–32.

The idea behind MSM is to represent the charged object as a collection of spheres then compute the forces between each sphere, as well as the torque they generate. The sum of these forces and torques is the net force and torque experienced by the spacecraft. For this work, it is assumed the spacecraft are fully conducting: the electric potential on the target surface is uniform and the potential of each sphere is the same. Having a fully conducting outer surface is a common GEO satellite requirement to mitigate differential charging. The charge on each sphere is then computed knowing the sphere size and location; because these spheres are all in close proximity, there is capacitance coupling that must be accounted for. Equation (1) shows the method for computing the voltage of a single sphere given N_T total spheres

$$V_i = \frac{1}{4\epsilon_0\pi}\frac{Q_i}{R_i} + \sum_{\substack{k=1\\k\neq i}}^{N_T}\left[\frac{1}{4\epsilon_0\pi}\frac{Q_k}{r_{i,k}}\right] \tag{1}$$

with Q_i and R_i as the charge and radius of sphere i, and $r_{i,k}$ is the separation distance between spheres i and k. The permeability of free space is represented by ϵ_0. This summation can be represented in matrix form, which allows for easy computation of all Q_i's:

$$\begin{bmatrix} V_1 \\ V_2 \\ \vdots \\ V_N \end{bmatrix} = \underbrace{\frac{1}{4\epsilon_0\pi}\begin{bmatrix} \frac{1}{R_1} & \frac{1}{r_{1,2}} & \cdots & \frac{1}{r_{1,N}} \\ \frac{1}{r_{2,1}} & \frac{1}{R_2} & \cdots & \frac{1}{r_{2,N}} \\ \vdots & \vdots & \ddots & \vdots \\ \frac{1}{r_{n,1}} & \frac{1}{r_{n,2}} & \cdots & \frac{1}{R_N} \end{bmatrix}}_{S}\begin{bmatrix} Q_1 \\ Q_2 \\ \vdots \\ Q_N \end{bmatrix}. \tag{2}$$

Here, S is the $N \times N$ elastance matrix. With the equation of the form $[V] = [S][Q]$, the elastance matrix can be inverted to the capacitance matrix and $[Q]$ is computed using the known voltage matrix. The spacecraft size and location are inputs, so R_i and $r_{i,k}$ are known for all spheres. Because this requires inverting an $N \times N$ matrix, the computation time increases with number of spheres.

With the charge on each sphere computed, the net torque is determined by computing the force between two spheres and taking the cross product between the separation vector and sphere location vector. This value is computed between each sphere pair and summed to get the net torque about the object's center of mass. For a servicer represented by N_S spheres and a target of N_T spheres, the net torque acting on the servicer is computed as

$$\boldsymbol{L}_S = \frac{1}{4\epsilon_0 \pi} \sum_{i=1}^{N_S} q_i \sum_{k=1}^{N_T} \left[\frac{q_k}{r_{i,k}^3} \boldsymbol{r}_i \times \boldsymbol{r}_{i,k} \right], \tag{3}$$

where $\boldsymbol{r}_i$ is the location of sphere i with respect to the servicer's center of mass.

Figure 2 shows the two spacecraft used in this paper represented by the MSM. For this work, the servicer is a bus and single paneled spacecraft, similar to the GOES-R spacecraft, consisting of 72 spheres. The target is a two panel spacecraft represented by the SSL-1300 spacecraft bus and is made of 92 spheres. These spacecraft geometries and MSM representations are chosen to be consistent with prior work both exploring EMM and electrostatic detumbling. In Fig. 2, the color

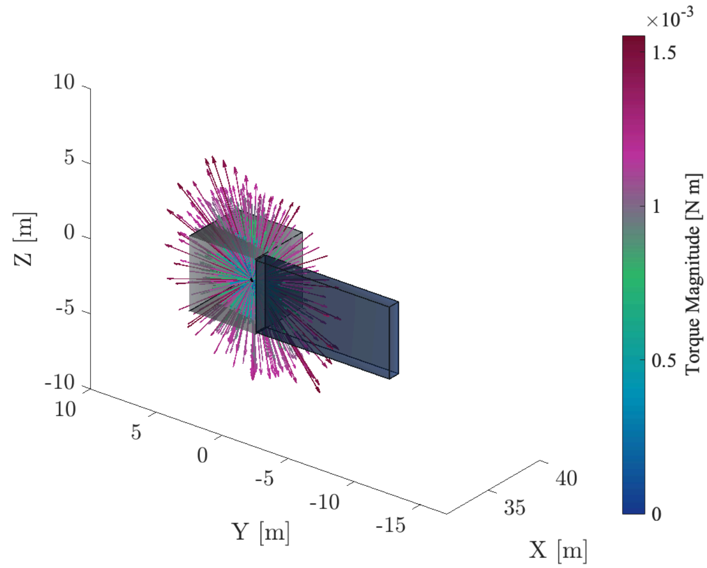

Figure 3. All computed torques for a constant servicer attitude with $n = 10$

bar corresponds to the charge density of spheres. It can be seen that the large densities, and therefore higher charges, occur at the ends of the thin solar panels on both spacecraft. Because the charges are greater and are typically further from the spacecraft center of mass, these regions have the most significant effect on electrostatic torque generation.

To determine the attitude that generates an electrostatic torque opposite the stored angular momentum vector, a database of torques is built. A total of n^3 servicer attitudes are considered using 3-2-1 Euler angles varying between -180°:$\frac{180}{n}$:180°, -90°:$\frac{90}{n}$:90°, and -180°:$\frac{180}{n}$:180° respectively.

For these simulations, $n = 9$ is used and has achieved similar results to $n = 50$. The electrostatic torque at each attitude is computed and stored. This database considers a fixed separation distance, servicer/target potentials, and target attitude. Figure 3 shows all the torques the servicer can experience for the target attitude shown in Fig. 2.

These computed torques act in multiple directions with the significant components being about the ${}^{\mathcal{N}}\hat{\text{Y}}$ and ${}^{\mathcal{N}}\hat{\text{Z}}$ axes. This suggests that the servicer will have the most control authority (with respect to dumping momentum) about these two axes. An important factor to consider is that two reference frames are considered in this paper: the inertial reference frame denoted by the superscript $\mathcal{N}$ and the servicer's body frame indicated by the superscript $\mathcal{B}$. In Fig. 2, the two frames are aligned with the plot axes.

Electrostatic Momentum Transfer

The rate of change of the angular momentum of a rigid body about the center of mass is given by[33]

$$\dot{\boldsymbol{H}} = \boldsymbol{L}, \tag{4}$$

where $\boldsymbol{L}$ is the net external torque experienced by the body. By applying an external torque, the angular momentum can be increased or decreased. This is the driving idea behind EMM: by generating an $\boldsymbol{L}_{\text{elec}}$ whose sign is opposite that of the servicer's angular momentum vector, the magnitude of $\boldsymbol{H}$ will decrease, decreasing reaction wheel speeds.

The process of EMM is as follows. The servicer maintains the first attitude, performing the science/maneuver required for the mission. While this attitude is maintained, both spacecraft experience electrostatic torques: the servicer stores the increasing angular momentum in reaction wheels while the uncontrolled debris object begins to tumble. The reaction wheels spin up to store this angular momentum and once they reach a pre-determined threshold, they begin the EMM de-saturation maneuver.

First, the second, anti-parallel torque attitude must be determined by searching the pre-computed torque database. The normalized dot product between the servicer's angular momentum and each electrostatic torque is computed and the minimum normalized dot product gives the most opposite torque (and the corresponding attitude). However, only using this criteria leads to cases with small torques and long de-saturation times. To account for this, the torque direction is weighted 10-to-1 to its magnitude to ensure quick de-saturation times. With the second attitude computed, the servicer then slews to the new attitude. This slew is governed by a motor torque optimal reaction wheel control law using modified Rodriguez parameters [33, Ch. 8.7]. After the second attitude is achieved, the servicer holds this attitude until the reaction wheels have reduced their speeds as much as possible. Finally, the servicer begins its slew back to the first attitude, using the same motor torque control. The first attitude is then maintained until the reaction wheels exceed the threshold and the process continually repeats.

CONTINUOUS MOMENTUM MANAGEMENT WITH A ROTATING TARGET

A simulation framework using the methods described in the previous section is designed and implemented here. The spacecraft are charged to ± 10 kV (positive servicer/negative target) and maintain a constant 30 m separation distance between the spacecraft center of mass. These potentials are the order of magnitude required for EA and a 30 m separation distance ensures the two spacecraft will not collide. Translation dynamics are not explored here and the separation distance

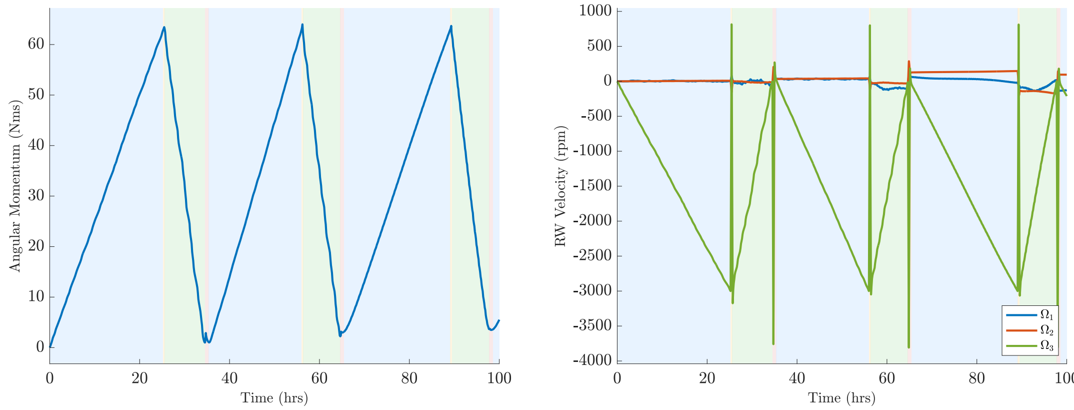

(a) Magnitude of angular momentum (b) Reaction wheel speeds

Figure 4. Using electrostatic momentum management to combat increasing wheel speeds over 100 hours.

is assumed to remain fixed with a complementary relative position control system. Starting with both spacecraft initially at rest and reaction wheel speeds of zero, the servicer maintains the desired attitude presented in Fig. 2. Figure 4 shows the angular momentum magnitude and the reaction wheel speeds of the servicer over 100 hrs implementing EMM. An RW saturation limit of 6000 rpm is considered, but because reaction wheels are used for attitude control, a wheel speed threshold of 3000 rpm is used to prevent wheel saturation during the slews and avoid possible loss of control due the RW gyroscopic requirement.

In these figures, there are four colored regions, each corresponding to a different phase in the maneuver. Blue and green indicate when the servicer is maintaining the first and second attitudes respectively. The yellow and red regions represent when the spacecraft is slewing between attitudes. Over these first 100 hours, the angular momentum magnitude oscillates between 0 and 64 Nms. The angular momentum does not completely reach 0 Nms but gets close. This occurs because the target is rotating and the computed anti-parallel torque is not the exact torque it experiences. Additionally, the servicer experiences electrostatic torques during the slew, which also alter the direction of the angular momentum vector. From Fig. 4(b), the dominant torque is about the inertially-fixed axis ${}^{\mathcal{N}}\hat{\mathrm{Z}}$. This is expected because with the configuration in Fig. 2, the charge concentrations are at the edges of the solar panels and the ${}^{\mathcal{N}}\hat{\mathrm{X}}$ and ${}^{\mathcal{N}}\hat{\mathrm{Y}}$ torques should be small. Another important aspect is, while the de-saturation threshold is chosen as 3000 rpm, it can be seen that the ${}^{\mathcal{B}}\hat{\mathrm{Z}}$-axis reaction wheel exceeds this threshold. Because the reaction wheels are also being used to perform the slew, they need to further spin up to generate the required torques to rotate the large spacecraft. However, even with wheel speeds near 4000 rpm, they do not approach the saturation limit of 6000 rpm.

Extending the simulation time to 1000 hrs, the long term momentum behavior can be examined. The simulation shown in Fig. 5 is conducted for 1000 hrs simulation time. Over the full 1000 hours, the angular momentum is kept below 64 Nms and the wheel speeds do not approach the 6000 rpm limit. This suggests that, even with the rotating target, reaction wheels can be kept from reaching the saturation limit purely using electrostatic torques. However, while the wheel speeds are kept bounded, there is a buildup of angular momentum. This "un-dumped" angular momentum is in the ${}^{\mathcal{B}}\hat{\mathrm{X}}$ and ${}^{\mathcal{B}}\hat{\mathrm{Y}}$ wheels. A continued buildup of momentum will eventually cause the reaction wheels

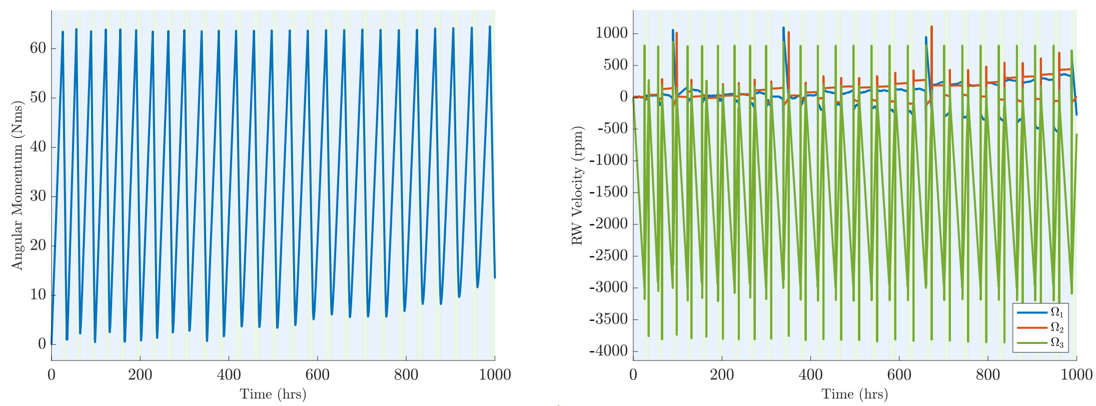

(a) Magnitude of angular momentum (b) Reaction wheel speeds

Figure 5. Using electrostatic momentum management to combat increasing wheel speeds of a 1000 hours.

to saturate: additional momentum management techniques are needed to fully spin down reaction wheels. However, without EMM, over the course of 1000 hrs, a ΔH of ≈1640 Nms would need to be removed by thrusters with 26 separate burns. Using EMM, this ΔH is only 13 Nms and thrusters would not have to be fired in the 1000 hour time frame.

Angular Momentum about the Principal Axes

To explore the need for thrusters or alternate momentum management techniques, this paper looks at the ability of the servicer to manage momentum about each principal axis: if a torque that acts purely in the ${}^{\mathcal{N}}\hat{\text{Y}}$ axes can be generated, then momentum buildup about the ${}^{\mathcal{N}}\hat{\text{Y}}$ axis can be removed. This is explored by initializing the target with a reaction wheel speed of ±3000 rpm about each of the ${}^{\mathcal{B}}\hat{\text{X}}$, ${}^{\mathcal{B}}\hat{\text{Y}}$, and ${}^{\mathcal{B}}\hat{\text{Z}}$ axes. Starting with the ${}^{\mathcal{B}}\hat{\text{Z}}$-axis case, Fig. 6 shows the two cases where the servicer is initialized with angular momentum about either the +${}^{\mathcal{N}}\hat{\text{Z}}$ or -${}^{\mathcal{N}}\hat{\text{Z}}$ directions. The shaded regions correspond to the same maneuver phases as Fig. 4.

As expected, regardless of the initial direction of the ${}^{\mathcal{N}}\hat{\text{Z}}$-axis angular momentum, an opposite torque can be produced to spin down the reaction wheels. Additionally, the generated torque is (almost) purely about the ${}^{\mathcal{N}}\hat{\text{Z}}$-axis in both cases, so the other reaction wheels do not spin up. One interesting factor that can be seen in Fig. 6(c) is that the reaction wheel velocity starts at +3000 rpm, but after the slew, the reaction wheel velocity is negative. This occurs because the best torque, according to the weights, actually occurs when the spacecraft is flipped ≈180° about the ${}^{\mathcal{N}}\hat{\text{Y}}$-axis first.

Now considering an angular momentum vector about the ${}^{\mathcal{N}}\hat{\text{Y}}$-axis, the servicer is still initialized at the first attitude, but the ${}^{\mathcal{B}}\hat{\text{Y}}$-axis reaction wheel has a ±3000 rpm initial speed. Fig. 7 shows these two cases. Similar to before, starting with an angular momentum vector purely about the inertial frame ${}^{\mathcal{N}}\hat{\text{Y}}$-axis, a servicer attitude can be achieved such that the reaction wheels are able to reach near 0 values. As opposed to trials shown in Fig. 6, the wheel velocities get reallocated during the slew. Initially, only the ${}^{\mathcal{B}}\hat{\text{Y}}$-axis has a non-zero reaction wheel speed, but to achieve the desired second attitude, the ${}^{\mathcal{B}}\hat{\text{Z}}$-axis has to spin up. Because of this, the resulting reaction wheel velocity plots appear similar to those in Fig. 6. This behavior is true for both ±${}^{\mathcal{N}}\hat{\text{Y}}$-axis trials.

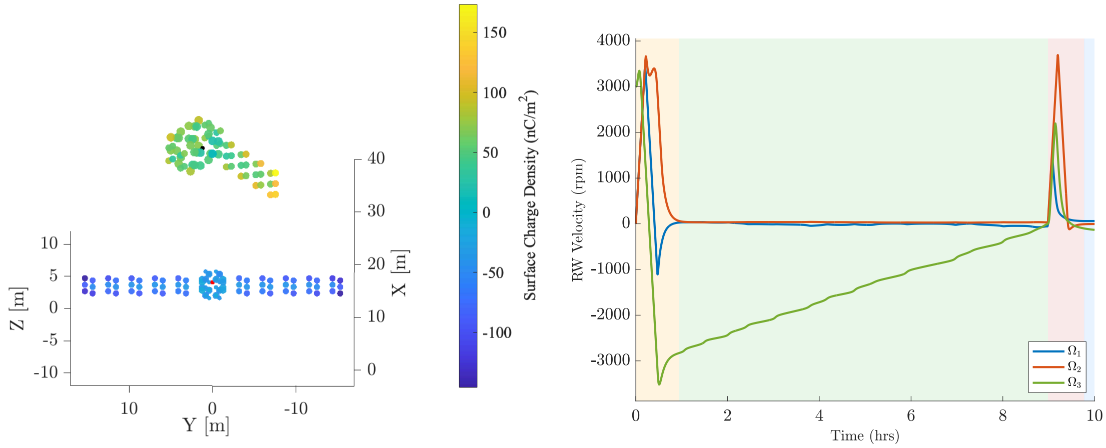

(a) Anti-parallel attitude starting with pure +$^{\mathcal{N}}\hat{Z}$ angular momentum

(b) Reaction wheel speeds starting with pure +$^{\mathcal{N}}\hat{Z}$ angular momentum

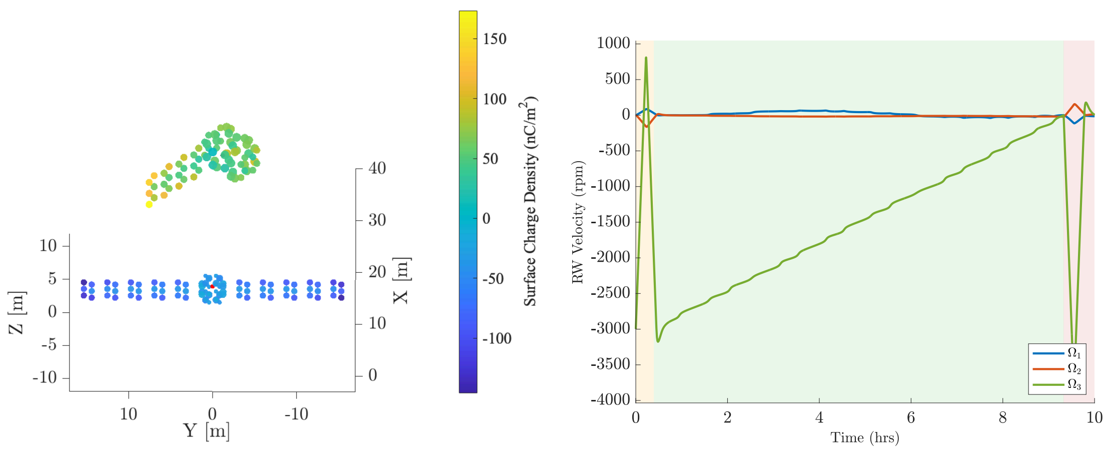

(c) Anti-parallel attitude starting with pure -$^{\mathcal{N}}\hat{Z}$ angular momentum

(d) Reaction wheel speeds starting with pure -$^{\mathcal{N}}\hat{Z}$ angular momentum

Figure 6. The wheel spin down portion of an EMM maneuver with pure angular momentum about the $^{\mathcal{N}}\hat{Z}$-axis.

Based on Fig. 3, the possible torques experienced by the servicer form a plane in the $^{\mathcal{N}}\hat{Y}$-axis/$^{\mathcal{N}}\hat{Z}$-axis plane. In many of the torques, there is a noticeable $^{\mathcal{N}}\hat{X}$-axis component; however, it is never the case where the $^{\mathcal{N}}\hat{X}$-axis is the major component. The result of this, when starting with an angular momentum about the $\pm^{\mathcal{N}}\hat{X}$-axis, is that an anti-parallel torque cannot be achieved. Searching the torque data with both these initial wheel speeds, the minimum dot product is -0.137. While there is an $^{\mathcal{N}}\hat{X}$-axis component, the torque vector is still nearly perpendicular to the angular momentum vector. Because of this, it is difficult for pure $^{\mathcal{N}}\hat{X}$-axis momentum to be managed with the current satellite configuration.

When only considering electrostatic perturbations (for this configuration), all of the torques are mainly about the $^{\mathcal{N}}\hat{Y}$-axis and $^{\mathcal{N}}\hat{Z}$-axis: the $^{\mathcal{N}}\hat{X}$-axis momentum will grow slowly relative to the other axes. It will take a considerable amount of time for the wheel to saturate, which could be extended by including redundant reaction wheels. However, eventually, a thruster burn would be

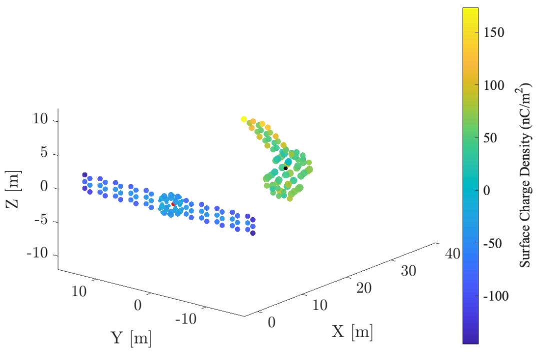

(a) Anti-parallel attitude starting with pure +$^{\mathcal{N}}\hat{\text{Y}}$ angular momentum

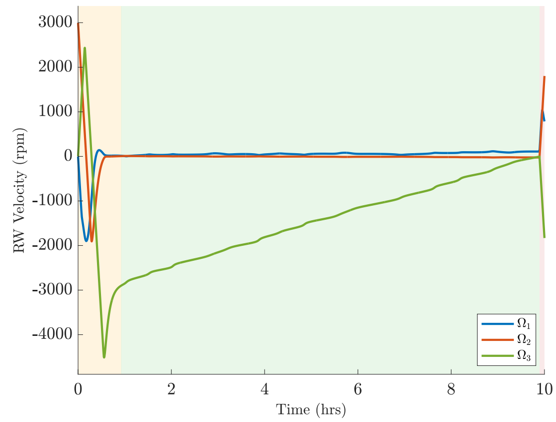

(b) Reaction wheel speeds starting with pure +$^{\mathcal{N}}\hat{\text{Y}}$ angular momentum

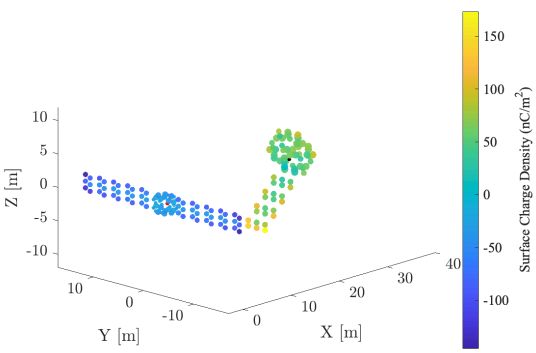

(c) Anti-parallel attitude starting with pure -$^{\mathcal{N}}\hat{\text{Y}}$ angular momentum

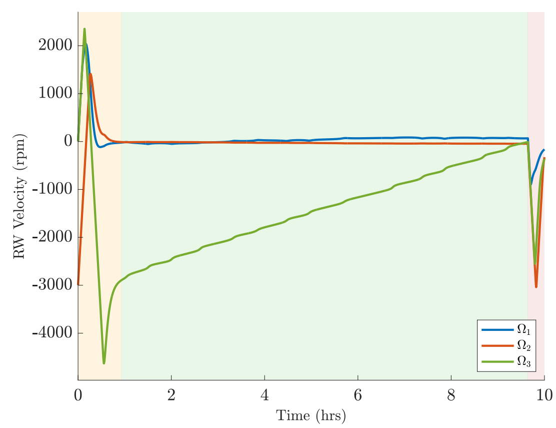

(d) Reaction wheel speeds starting with pure -$^{\mathcal{N}}\hat{\text{Y}}$ angular momentum

Figure 7. The wheel spin down portion of an EMM maneuver with angular momentum about the $^{\mathcal{N}}\hat{\text{Y}}$-axis.

required to remove the $^{\mathcal{N}}\hat{\text{X}}$-axis momentum. This behavior presents a limitation of EMM: there is no guarantee that an electrostatic torque can be generated for an arbitrary momentum vector. The efficiency of EMM will depend on the geometries of both the target and servicer and depending on these shapes, thrusters may also be required to manage the spacecraft's momentum.

SERVICER ATTITUDE EFFECTS

Because the computed torques will not be identical to the those experienced when considering a rotating target, there will be a more significant buildup of angular momentum. This behavior can be explored by looking at the torques experienced by the servicer at the first and second attitudes. Varying the target's attitude, the possible torques experienced by the servicer are computed and shown in Fig. 8. While the second attitude is re-determined for each de-saturation maneuver, the general attitude will be consistent when the $^{\mathcal{N}}\hat{\text{Z}}$-axis dominates the angular momentum vector.

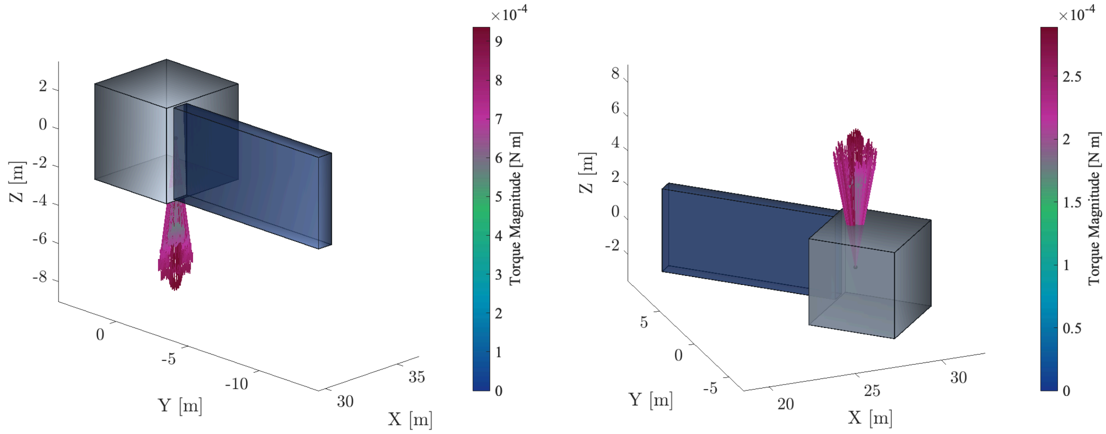

(a) First attitude

(b) Second Attitude

Figure 8. The electrostatic torques experienced by the servicer for 729 different target attitudes.

At the first attitude, all the experienced torques are predominantly in the -${}^{\mathcal{N}}\hat{\text{Z}}$ direction regardless of servicer attitude; there are noticeable ${}^{\mathcal{N}}\hat{\text{X}}$ and ${}^{\mathcal{N}}\hat{\text{Y}}$ components that create a narrow distribution of torques, but they are small compared to the ${}^{\mathcal{N}}\hat{\text{Z}}$-axis component. This is due to the solar panel being the dominant contributor to the electrostatic torque: the thin panel has the largest charge concentrations and has the largest distance from the spacecraft's center of mass. This same behavior is seen at the second attitude, except the distribution is about the +${}^{\mathcal{N}}\hat{\text{Z}}$ direction. By only switching between these two (or similar) attitudes, the electrostatic torques are kept mainly about the ${}^{\mathcal{N}}\hat{\text{Z}}$-axis regardless of the target's attitude. For the configuration shown here, the target rotation has a limited effect on the efficiency of EMM. However, this behavior is dependent on the servicer's attitude.

Continuing this analysis for additional servicer attitudes, a pattern can be seen. Figure 9 rotates the servicer with a yaw angle ranging from -80° to -105°. At each angle, the target attitude is varied and the distribution of torques is plotted.

As the spacecraft panel gets closer to the target (the yaw angle approaches -90°), the distribution of forces becomes wider. At -80° and -105° the majority of torques are grouped around the ${}^{\mathcal{N}}\hat{\text{Z}}$-axis, but as the yaw angle approaches -90°, the experienced torques fill out the ${}^{\mathcal{N}}\hat{\text{Y}}$/${}^{\mathcal{N}}\hat{\text{Z}}$ plane. There is not one major direction and the experienced torques are different than the pre-computed values. As the yaw angle goes to 0° and -180°, the distribution of torques becomes significantly more narrow.

Given that the highest charge concentrations are on the solar panel, this may be caused by small changes in attitude when the target's solar panels are close to the servicer's. The large charges and small separation distances would create sensitive electrostatic torques. This can be tested by evaluating the torque distributions when the servicer solar panel is pointed away from the target. Figure 10 rotates the servicer with a yaw angle ranging from 70° to 110°.

With the panel pointed away from the target, there is still a wide distribution of torques for yaw angles between 70° to 110°. Similar to before, as the yaw angles approach either 0° or 180°, the distribution becomes more narrow, only now the charge concentrations are far from the target. In fact, the distributions appear to be more diffuse at these attitudes, with a larger range of angles having wide torque distributions. By comparing Figs. 9 and 10, the commonality is seen to be that wide torque distributions occur when the servicer is relatively symmetric to the target.

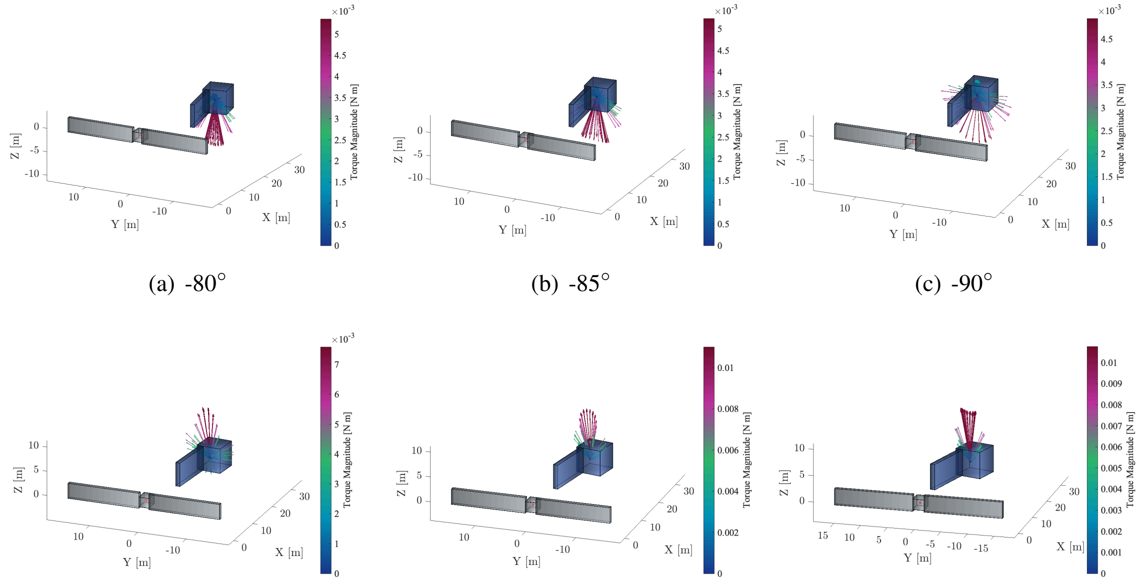

(a) -80° (b) -85° (c) -90°

(d) -95° (e) -100° (f) -105°

Figure 9. All torques experienced by the servicer with negative yaw angles (about $^{\mathcal{N}}\hat{\mathbf{Z}}$).

When the servicer has its panel aligned with the $^{\mathcal{N}}\hat{\text{Y}}$-axis, regardless of the servicer's attitude, the resulting force on the object will pull the panel towards the target. This is because the location of the panel dominates the generated torque: it extends far enough from the target such that the panel can only be pulled counterclockwise about the $^{\mathcal{N}}\hat{\text{Z}}$-axis. When the servicer's panel is pointed toward or away from the target, this is no longer the case. The symmetry of the servicer now allows it to be pulled either clockwise or counterclockwise about the $^{\mathcal{N}}\hat{\text{Z}}$-axis or even about the $^{\mathcal{N}}\hat{\text{Y}}$-axis. Figure 11 shows a simple case of this, with a -90° yaw angle for the servicer and $\pm 45°$ yaw angle for the target

Even though the majority of the target body is on the left side of the center of mass of the servicer, the resulting torque is in the $^{\mathcal{N}}\hat{\text{Z}}$ direction. This is because the highly charged target solar panel has a smaller separation from the target's solar panel and pulls the spacecraft counterclockwise much stronger than the rest of the target body. The same behavior is true when the target has a -45° yaw angle, albeit flipped directions. Only two directions are shown here, but this behavior occurs across a range of target attitudes.

CONCLUSION

The goal of this paper is to demonstrate electrostatic momentum management (EMM) considering a rotating target and determine the relationship between servicer attitude and the robustness of EMM. To perform electrostatic momentum management, a database of possible electrostatic torques is computed for every servicer attitude. Because this database is built considering a stationary target, as the target rotates, the resulting torque experienced by the servicer changes and the expected torque differs from the actual experienced torque. This can lead to a consistent increase in angular momentum. If this buildup occurs about an axis that torques can not easily be generated about, other momentum management techniques, such as chemical thrusters, may still be needed. However, em-

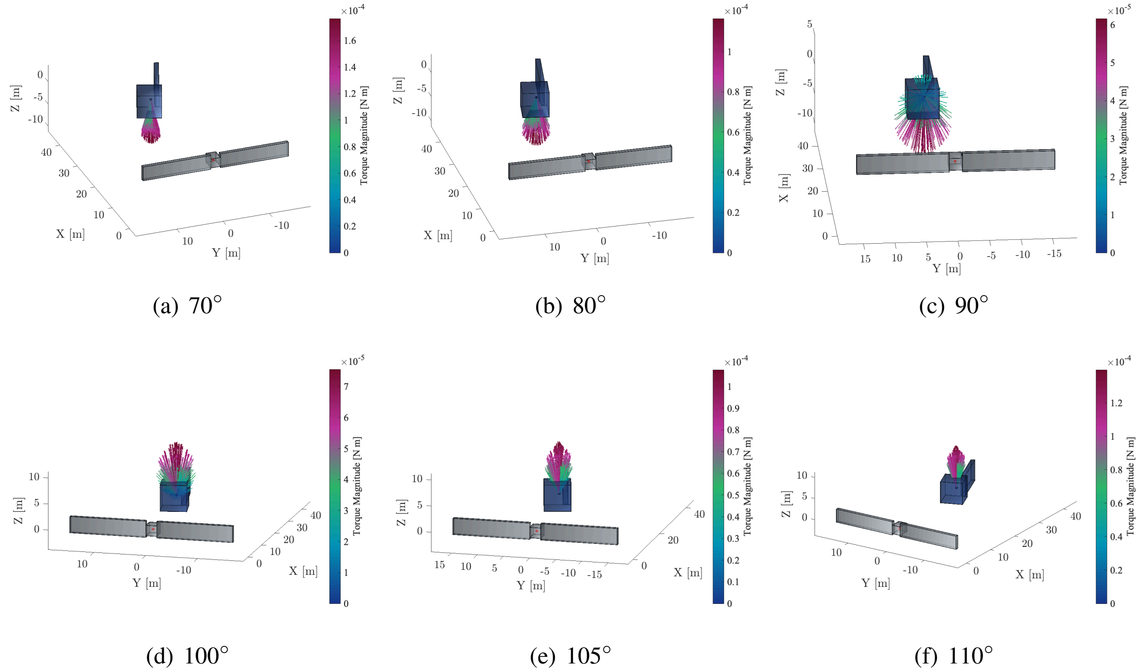

(a) 70°   (b) 80°   (c) 90°

(d) 100°   (e) 105°   (f) 110°

Figure 10. All torques experienced by the servicer with positive yaw angles (about $^{\mathcal{N}}\hat{\mathbf{Z}}$).

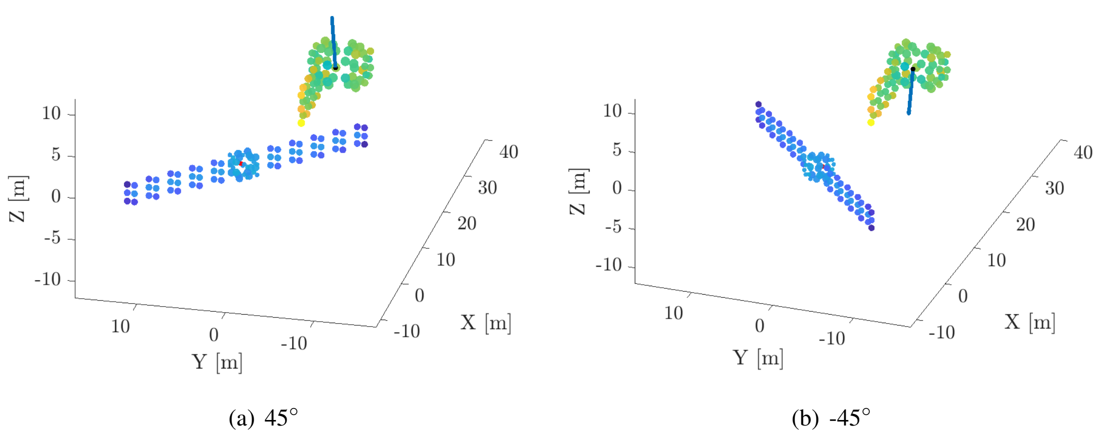

(a) 45°   (b) -45°

Figure 11. The torques experienced by the servicer when the target has a $\pm 45°$ yaw angle (about $^{\mathcal{N}}\hat{\mathbf{Z}}$).

ploying electrostatic momentum management reduces the frequency of burn maneuvers, extending the lifetime of potential missions.

This buildup is mainly caused by the inconsistencies between the precomputed database and the actual experienced torques. To characterize this, the distribution of torques experienced by a servicer at a variety of attitudes is evaluated. These errors occur when the servicer is relatively symmetric in the ${}^{\mathcal{N}}\hat{\text{Y}}$/${}^{\mathcal{N}}\hat{\text{Z}}$ plane, the view from the center of mass of the target. This symmetry allows torques to be generated about in multiple directions as the target rotates. When the view is asymmetric, on the other hand, the torque directions are consistent. The charge concentrations on the solar panel dominate the behavior and extend in a direction such that the panel can only be pulled inward, regardless of the target's attitude.

The servicing spacecraft can be constructed to have a strong asymmetry to increase the attitudes with consistent torque generation, but there is no guarantee that the torque distribution for a given servicer attitude will only point in a single direction. If the servicer maintains one of these attitudes, angular momentum management will not be effective using electrostatic torques. To improve the robustness of EMM to rotating targets, these attitudes must be identified and removed as candidate attitudes. These attitudes have been identified for the current spacecraft geometry and can now be avoided, but this behavior may vary when considering different satellite configurations. Future work will develop methods for identifying these "non-robust" attitudes for arbitrary spacecraft geometries and removing them from the database of possible servicer attitudes.

ACKNOWLEDGMENTS

This project was supported by the Department of Defense (DoD) through the National Defense Science and Engineering Graduate (NDSEG) Fellowship Program.

REFERENCES

[1] S. T. Lai, *Fundamentals of Spacecraft Charging*. Princeton University Press, Oct. 2011, 10.2307/j.ctvcm4j2n.

[2] L. B. King, G. G. Parker, S. Deshmukh, and J. H. Chong, "Study of interspacecraft Coulomb forces and implications for formation flying," *Journal of Propulsion and Power*, Vol. 19, No. 3, 2003, pp. 497–505, 10.2514/2.6133.

[3] H. Schaub, G. G. Parker, and L. B. King, "Challenges and Prospect of Coulomb Formations," *Journal of the Astronautical Sciences*, Vol. 52, Jan.–June 2004, pp. 169–193.

[4] K. Wilson and H. Schaub, "Impact of Electrostatic Perturbations on Proximity Operations in High Earth Orbits," *Journal of Spacecraft and Rockets*, Vol. 58, No. 5, 2021, pp. 1–10, 10.2514/1.a35039.

[5] K. Wilson and H. Schaub, "Constrained guidance for spacecraft proximity operations under electrostatic perturbations," *IEEE Aerospace Engineering Conference*, Big Sky, MT, Mar. 2021, pp. 1–11.

[6] K. T. H. Wilson, A. Romero Calvo, and H. Schaub, "Constrained Guidance for Spacecraft Proximity Operations Under Electrostatic Perturbations," *Journal of Spacecraft and Rockets*, Vol. 59, July–Aug. 2022, pp. 1304–1316, 10.2514/1.A35162.

[7] T. Bennett and H. Schaub, "Contactless electrostatic detumbling of axi-symmetric GEO objects with nominal pushing or pulling," *Advances in Space Research*, Vol. 62, Dec. 2018, pp. 2977–2987, 10.1016/j.asr.2018.07.021.

[8] F. Casale, H. Schaub, and J. Douglas Biggs, "Lyapunov Optimal Touchless Electrostatic Detumbling of Space Debris in GEO Using a Surface Multisphere Model," *Journal of Spacecraft and Rockets*, May 2021, pp. 1–15, 10.2514/1.A34787.

[9] H. Schaub and D. Stevenson, "Prospects of Relative Attitude Control Using Coulomb Actuation," *The Journal of the Astronautical Sciences*, Vol. 60, Dec. 2013, pp. 258–277, 10.1007/s40295-015-0048-y.

[10] V. Aslanov and H. Schaub, "Detumbling Attitude Control Analysis Considering an Electrostatic Pusher Configuration," *Journal of Guidance, Control, and Dynamics*, Vol. 42, Apr. 2019, pp. 900–909, 10.2514/1.G003966.

[11] D. Stevenson and H. Schaub, "Electrostatic spacecraft rate and attitude control—Experimental results and performance considerations," *Acta Astronautica*, Vol. 119, Feb. 2016, pp. 22–33, 10.1016/j.actaastro.2015.10.023.

[12] H. Schaub and D. F. Moorer, "Geosynchronous Large Debris Reorbiter: Challenges and Prospects," *The Journal of the Astronautical Sciences*, Vol. 59, No. 1–2, 2014, pp. 161–176, 10.1007/s40295-013-0011-8.

[13] D. F. Moorer and H. Schaub, "Electrostatic spacecraft reorbiter," 2011a. US Patent 8,205,838 B2.

[14] D. F. Moorer and H. Schaub, "Hybrid electrostatic space tug," 2011b. US Patent 0036951-A1.

[15] H. Schaub and D. F. Moorer, "Geosynchronous Large Debris Reorbiter: Challenges and Prospects," *The Journal of the Astronautical Sciences*, Vol. 59, Jun. 2012, pp. 161–176, 10.1007/s40295-013-0011-8.

[16] H. Schaub and Z. Sternovsky, "Active Space Debris Charging for Contactless Electrostatic Disposal Maneuvers," *Advances in Space Research*, Vol. 43, No. 1, 2014, pp. 110–118, 10.1016/j.asr.2013.10.003.

[17] H. Schaub and L. E. Z. Jasper, "Circular Orbit Radius Control Using Electrostatic Actuation for 2-Craft Configurations," *AAS/AIAA Astrodynamics Specialist Conference*, Girdwood, Alaska, July 31 – August 4 2011. Paper AAS 11–498.

[18] E. A. Hogan and H. Schaub, "Relative Motion Control For Two-Spacecraft Electrostatic Orbit Corrections," *Journal of Guidance, Control, and Dynamics*, Vol. 36, Jan. 2013, pp. 240–249, 10.2514/1.56118.

[19] J. D. Walker and H. Schaub, "Electron Gun-Based Active Charge Control of Nearby Spacecraft," *IEEE Transactions on Plasma Science*, 2025, pp. 1–15, 10.1109/TPS.2025.3627474.

[20] J. Walker and H. Schaub, "Development of Experimental Methods for Active Charge Control using Remote Sensing Methods," *Spacecraft Charging and Technology Conference*, Avignon, France, June 17–21 2024.

[21] F. B. Leahy, "Cross-Program Design Specification for Natural Environments (DSNE)," Tech. Rep. SLS-SPEC-159, NASA, 2021. `https://ntrs.nasa.gov/citations/20210024522`.

[22] K. Champion and H. Schaub, "Electrostatic Potential Shielding in Representative Cislunar Regions," *IEEE Transactions on Plasma Science*, Vol. 51, No. 9, 2023, pp. 2482–2500, 10.1109/TPS.2023.3236246.

[23] J.-F. Trégouët, D. Arzelier, D. Peaucelle, C. Pittet, and L. Zaccarian, "Reaction wheels desaturation using magnetorquers and static input allocation," *IEEE Transactions on Control Systems Technology*, Vol. 23, No. 2, 2014, pp. 525–539.

[24] F. Giulietti, A. A. Quarta, and P. Tortora, "Optimal control laws for momentum-wheel desaturation using magnetorquers," *Journal of guidance, control, and dynamics*, Vol. 29, No. 6, 2006, pp. 1464–1468.

[25] Y. Yang, "Spacecraft attitude and reaction wheel desaturation combined control method," *IEEE Transactions on Aerospace and Electronic Systems*, Vol. 53, No. 1, 2017, pp. 286–295.

[26] E. A. Hogan and H. Schaub, "Three-Axis Attitude Control Using Redundant Reaction Wheels with Continuous Momentum Dumping," *AIAA Journal of Guidance, Control, and Dynamics*, Vol. 38, Oct. 2015, pp. 1865–1871, 10.2514/1.G000812.

[27] K. Ü. Emri and O. Cihan, "Control Allocation of a GEO Satellite for Station-Keeping and Momentum Management by Using Thrusters and Reaction Wheels," *European Journal of Science and Technology*, No. 26, 2021, pp. 374–382, 10.31590/ejosat.958404.

[28] J. D. Walker, K. Champion, and H. Schaub, "Reaction Wheel Momentum Control While Electrostatically Tugging Tumbling Space Object," *AAS Astrodynamics Specialist Conference*, Broomfield, CO, Aug. 11–15 2024. Paper No. AAS 24-375.

[29] D. Stevenson and H. Schaub, "Multi-Sphere Method for modeling spacecraft electrostatic forces and torques," *Advances in Space Research*, Vol. 51, Jan. 2013, pp. 10–20, 10.1016/j.asr.2012.08.014.

[30] D. Stevenson and H. Schaub, "Optimization of Sphere Population for Electrostatic Multi Sphere Model," *IEEE Transactions on Plasma Science*, Vol. 41, Dec. 2013, pp. 3526–3535, 10.1109/TPS.2013.2283716.

[31] G. Ingram, J. Hughes, T. Bennett, C. Reilly, and H. Schaub, "Volume Multi-Sphere-Model Development Using Electric Field Matching," *Journal of Astronautical Sciences*, Vol. 65, No. 4, 2018, pp. 377–399, 10.1007/s40295-018-0136-x.

[32] J. A. Hughes and H. Schaub, "Heterogeneous Surface Multisphere Models Using Method of Moments Foundations," *Journal of Spacecraft and Rockets*, Vol. 56, Jul. 2019, pp. 1259–1266, 10.2514/1.A34434.

[33] H. Schaub and J. L. Junkins, *Analytical Mechanics of Space Systems*. Reston, VA: AIAA Education Series, 4th ed., 2018, 10.2514/4.105210.